A Study on Lateral Distribution of Implanted Ions in Silicon

Won Chae Jung[a]
Department of Electronic Engineering, Kyonggi University, Iui-dong, Yeongtong-gu, Suwon 443-760, Korea

Hyung Min Kim
Department of mechanical System Design Engineering, Kyonggi University, Iui-dong, Yeongtong-gu, Suwon 443-760, Korea

[a]E-mail : wcjung@kyonggi.ac.kr

(Received 13 March 2006, Accepted 28 June 2006)

Due to the limitations of the channel length, the lateral spread for two-dimensional impurity distributions is critical for the analysis of devices including the integrated complementary metal oxide semiconductor (CMOS) circuits and high frequency semiconductor devices. The developed codes were then compared with the two-dimensional implanted profiles measured by transmission electron microscope (TEM) as well as simulated by a commercial TSUPREM4 for verification purposes. The measured two-dimensional TEM data obtained by chemical etching-method was consistent with the results of the developed analytical model, and it seemed to be more accurate than the results attained by a commercial TSUPREM4. The developed codes can be applied on a wider energy range (1 KeV ~ 30 MeV) than a commercial TSUPREM4 of which the maximum energy range cannot exceed 1 MeV for the limited doping elements. Moreover, it is not only limited to diffusion process but also can be applied to implantation due to the sloped and nano scale structure of the mask.

Keywords : Implantation, Chemical etching, Computer simulation and developed model, TEM

1. INTRODUCTION

For the fabrication of CMOS devices, the source and drain regions can be formed by using BF_2, B, P and As implantations for p^+ and n^+ doping. For ultra-shallow junctions, BF_2 and As impurities are implanted, and the implanted wafers are annealed for the electrical activation in a N_2 ambient. As device sizes declines, the accurate control of channel length and depth is critical in CMOS process. A variety of implantation experiments were carried out and analyzed for one and two-dimensional profiles[1-5]. SRIM[6-11] and UT-MARLOWE[12,13] were used as a Monte Carlo simulation tools for one-dimensional amorphous and crystalline profiles, respectively. Two-dimensional distributions of implanted impurities were visualized by using chemical etching and electron holography[14-17], and the developed model was compared with two-dimensional simulation data obtained using TSUPREM4 [18,19]. In the simulation, all annealing processes were carried out using proper diffusion coefficients[20,21] for the exact spreading diffusion effects. The output data of developed analytical model concurred with the measured TEM data after furnace annealing. For the range calculations in the vertical direction, the following equations were used:

$$C(x) = C_{dose} \cdot f(x) \tag{1}$$

where C_{dose} is implanted dose, C(x) represents concentrations as a function of the depth x, and $f(x)$ is a normal distribution function. The four moments are defined as

$$R_p = \int_0^\infty x \cdot f(x) = \frac{\sum X_i \cdot C_i}{\sum C_i} \tag{2}$$

$$\Delta R_p = \sqrt{\int_0^\infty (x - R_p)^2 \cdot f(x) dx} = \sqrt{\frac{\sum (X_i - R_p)^2 \cdot C_i}{\sum C_i}} \tag{3}$$

$$\gamma = \frac{\int_0^\infty (x - R_p)^3 \cdot f(x) dx}{\Delta R_p^{\,3}} = \frac{\sum (X_i - R_p)^3 \cdot C_i}{\sum C_i \cdot \Delta R_p^{\,3}} \tag{4}$$

$$\beta = \frac{\int_0^{\infty}(x-R_p)^4 \cdot f(x)dx}{\Delta R_p{}^4} = \frac{\sum (Xi-Rp)^4 \cdot Ci}{\sum Ci \cdot \Delta Rp^4} \quad (5)$$

where the first moment R_p (projected average range) is the average range under normal implantation, the second moment ΔR_p (standard deviation) represents the width of profile, the third moment γ (skewness) indicates the asymmetry of the profile, and the fourth moment β (kurtosis) represents the extent of profile sharpness in the peak-concentration area. A gaussian profile has only two parameters due to symmetry, and the equation can be expressed as,

$$C(x) = \frac{C_{\text{dose}}}{\sqrt{2\pi}\Delta Rp}\exp\left(-\frac{1}{2}\left[\frac{x-R_p}{\Delta Rp}\right]^2\right) \quad (6)$$

The projected average range (R_p) of Gaussian profile is located near the peak concentration.

The equation of concentration distribution after annealing can be described by $\Delta R_p = \sqrt{(\Delta R_p{}^2 + 2Dt)}$ instead of ΔR_p in equation 6. In asymmetric cases, the implanted profile can be expressed by using the four moments described in Eq. (2)-(5). For the gaussian profiles, the two parts of the profile in layer 1 and substrate 2 can be expressed[22,23] as,

$$C_1(x) = \frac{C_{dose}}{\sqrt{2\pi}\Delta R_{p1}} \cdot \exp[-\frac{(R_{p1}-x)^2}{2\Delta R_{p1}{}^2}]$$
$$0 < x < d \quad (7)$$

$$C_2(x) = \frac{C_{dose}}{\sqrt{2\pi}\Delta R_{p1}} \cdot \exp[-\frac{(d+(R_{p1}-d)\cdot\frac{\Delta R_{p2}}{\Delta R_{p1}}-x)^2}{2\Delta R_{p2}{}^2}]$$
$$x > d \quad (8)$$

where d is the thickness of the mask layer.

2. DEVELOPMENT OF ANAYTICAL MODEL OF TWO-DIMENSIONAL SIMULATION PROFILES

The developed program with an analytical description method is represented schematically in a flowchart in Fig. 1. From the Fig. 1, LAE and CGM denotes Linear Algebraic Equation and Conjugate Gradient Method, respectively. Grid, or simulation mesh in a 1D simulator is regular and easy to generate, however in 2D simulators, the mesh generation is much more difficult to

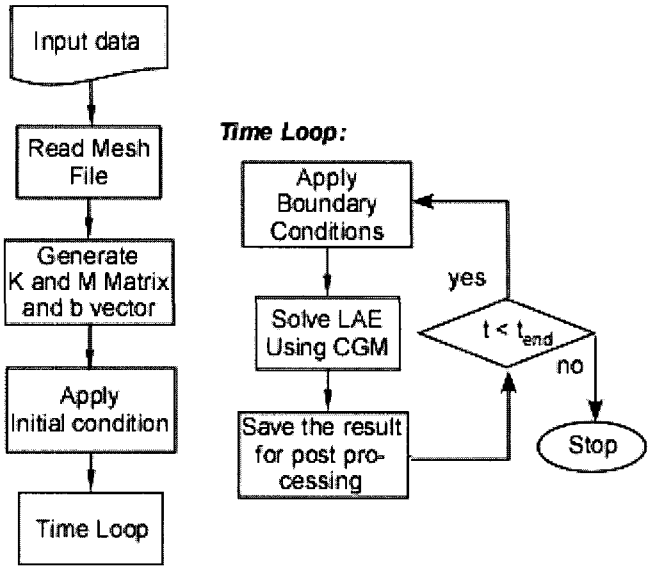

Fig. 1. Flow chart is depicted for the developed program.

construct. In order to reduce the time required for computation, a dense grid was used where abrupt changes were expected, and a sparse grid was used in circumstances where the gradients were not steep. Rectangular grids showed a better resolution of 2D profiles at corner areas between mask and substrate than rectangular grids and the calculated moments of simulated and SIMS data were inserted into analytical model in order to obtain 1D and 2D doping profiles.

The two-dimensional profile of the Gauss model can be described as

$$C(x,y) = C_{vert} \times \frac{1}{\sqrt{2\pi}\Delta R_y}\exp\left(-\frac{y^2}{2\Delta R_y{}^2}\right) \quad (9)$$

where C_{vert} is the vertical concentration, y is the lateral position and ΔR_y denotes the standard deviation of the lateral direction. For the two-dimensional profile of the Gauss model, equation 9 describes the results of implanting at a single point on the surface. For the implantation through a mask window, the doping profile can be calculated by superposition of a single point-response function and Eq. 9 can be express as

$$C(x,y) = C_{vert} \times C_{lateral}(y) = C_{vert} \times \frac{1}{2} \times$$
$$[erfc(\frac{y-a}{\sqrt{2}\cdot\Delta R_y}) - erfc(\frac{y+a}{\sqrt{2}\cdot\Delta R_y})] \quad (10)$$

where a is the mask window with an opening from y= -a to y=a for the lateral direction.

For high integrated circuits, the lateral standard deviation must consider for the devices of sub-micron size and corresponding equations of developed analytical model can be expressed as

$$C(x,y)=\frac{C_{dose}}{\sqrt{2\pi}\Delta R_p}\cdot\frac{1}{2C_t}\cdot\exp[\frac{-(y\tan\theta_t-(x-R_p))^2}{2\Delta R_p{}^2C_t{}^2}]\times$$
$$[1-erf(\frac{y+\tan\theta_t(\frac{\Delta R_y}{\Delta R_p})^2\cdot(x-R_p)}{\sqrt{2}\Delta R_y\cdot C_t}]+$$
$$\frac{1}{2C_m}\cdot\exp[\frac{-(-x\tan(\theta_m-\theta_t)-(x-R_p))^2}{2\Delta R_p{}^2\cdot C_m{}^2}]\times \quad (11)$$
$$[1-erf(\frac{-y+\tan(\theta_m-\theta_t)(\frac{\Delta R_y}{\Delta R_p})^2\cdot(x-R_p)}{\sqrt{2}\Delta R_y\cdot C_m})]$$

with

$$C_t=\sqrt{1+[\frac{\Delta R_y}{\Delta R_p}\cdot\tan\theta_t]^2}$$

$$C_m=\sqrt{1+[\frac{\Delta R_y}{\Delta R_p}\cdot\tan(\theta_m-\theta_t)]^2}$$

where the transformations of axes needed to describe the structure for tilt angles and mask angles can be expressed as

$$y=y'\cos\theta_t-x'\sin\theta_t,\quad x=x'\cos\theta_t-y'\sin\theta_t \quad (12)$$

3. EXPERIMENTS AND SIMULATIONS FOR TWO-DIMENSIONAL PROFILES

3.1 One- and two-dimensional profiles caused by As and BF_2 implantations in silicon

In this experiment, silicon wafers, (100) boron-doped n type with values of ρ of 1~3 Ωcm were used. For the source and drain doping for NMOS fabrication, 20-keV arsenic ions were implanted in silicon at 0° wafer tilt and a dose of 3.0×10^{15} cm^{-2}. The implanted and arsenic profiles were compared with the simulated data as depicted in Fig. 2. The data from the SIMS simulation corresponded with the UT-MARLOWE data and the SRIM data matched relatively well with the SIMS data with the exception for the tail region. The SRIM can be calculated using the range data for all amorphous material with every element, but the UT-MARLOWE can be calculated with the range data for amorphous and crystalline materials in limited elements. For a good statistical resolution of profiles, 100,000 ions were selected for SRIM and UT-MARLOWE simulations. The peak of the arsenic concentration by using SIMS is 7.13×10^{20} cm^{-3} at 0.0167 μm. The comparison from SIMS data and simulation data are shown in Table 1.

Table 1. Calculation of moments from different theoretical models and SIMS data for the arsenic implantation.

SIMS and Models	R_{peak} (μm)	R_p (μm)	ΔR_p (μm)	γ	β
SIMS data	0.0167	0.0137	0.0122	1.63	28.5
UT-MARLOWE	0.017	0.0193	0.0084	3.21	47.7
SRIM	0.0187	0.0203	0.0073	0.51	3.19

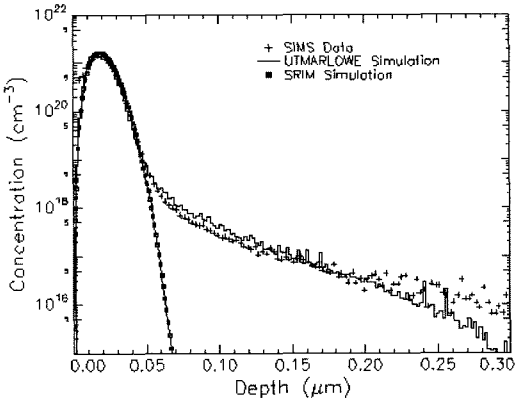

Fig. 2. Profiles of arsenic implanted profiles from the SIMS and the simulations.

TEM specimens for imaging impurity profiles can be suitable to delineate the doping contours, as published in several papers[15-17] by using selective chemical etching. Etching mixtures of HF: HNO_3: CH_3COOH (1: 20: 30) was used to selectively etch the cross-sectional TEM (XTEM) samples to reveal the doping distributions The nitric acid (HNO_3) oxidized the silicon, and the hydrofluoric acid (HF) dissolved the oxide. The acetic acid (CH_3COOH) acted as a dilution solution. For better resolution of 2D contour, a 500 W lamp illuminated the surface of the chemical solution from a distance 15 cm for 10 sec during the etching time. The etch rates depend on the doping concentration in the silicon substrate. The TEM images obtained by using chemical etching can provide useful and qualitative information on the two-dimensional extent of doping. The measured TEM data of the arsenic implantation were for a channel length and a vertical depth showed 83 nm and 237 nm, respectively. The bright region for the source and the drain is the etched region in comparison with the bulk-silicon region.

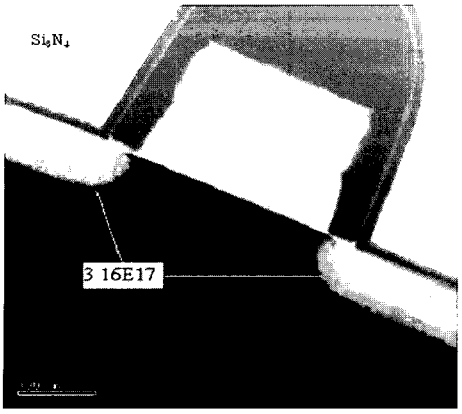

(a) Two-dimensional TEM image

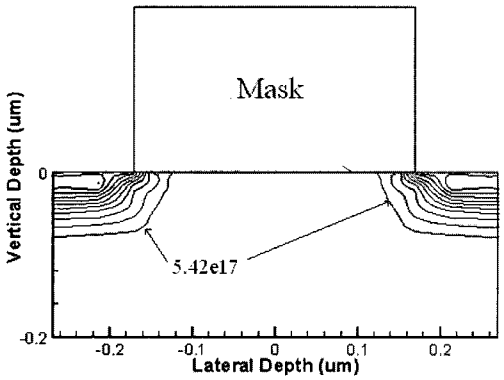

(b) Developed model

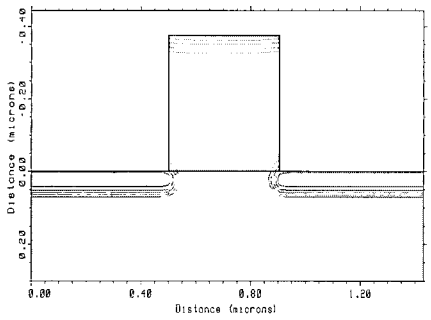

(c) TSUPREM4

Fig. 3. Two-dimensional TEM measurement and simulation of arsenic implanted silicon after annealing and chemical etching treatment(60,000× magnification).

The measured arsenic profile is compared with the simulated data for verification of 2D profiles of the source and the drain in Fig. 3. Sample preparations for the TEM measurements were carried out fast and easily using FIB (Focused Ion Beam) tool. For the experimental condition of the FIB, the beam current was 1-pA and the gallium ions as a source element were accelerated with 30-keV. The dose of the Ga^+ ion was 1.35×10^{19} cm^{-2} and the incident angle of the ions was 0 °. The trench dimensions were selected to be 3 μm×6 μm×

Table 2. TEM data after annealing compared with different simulation 2D-data in arsenic implanted silicon.

Model	Vertical depth (nm)	Channel length (nm)
Developed model	79	259
TSUPREM4	85.1	264.1
TEM	83	237

Table. 3. Calculation of moments from UT-MARLOWE and SIMS data for the BF_2 implantation.

Models	R_p (μm)	ΔR_p (μm)	γ	β
SIMS data	0.0195	0.0122	1.30	9.4
UT-MARLOWE	0.0193	0.0119	1.04	6.2

0.3 μm. Two-dimensional arsenic profile is measured by using TEM after annealing process and the magnification of the measured image was 60,000 in Fig. 3. The Nitride layer could be protected the mask during the chemical etching as depicted in Fig. 3.

In order to carry out the electrical activation, the wafers were furnace annealed for 15 min at 830 °C and rapidly thermal annealed for 10 sec at 980 °C in dry nitrogen. Under these annealing conditions, the arsenic diffusion coefficients were about 1.77×10^{-15} cm^2/s at 980 °C and 2.02×10^{-16} cm^2/s at 830 °C.

The two-dimensional distribution of annealed arsenic implanted silicon with mask is shown in Fig. 3. In this case, the channel length was 0.259 μm and the vertical depth was 79 nm, respectively. At the vertical depth of 79 nm, the concentration value of doping showed 5.42×10^{17} cm^{-3}. The comparison from TSUPREM4, TEM and developed model are shown in Table 2.

For the source and drain doping for PMOS fabrication, 20-keV BF_2 ions were implanted in silicon at 0 ° wafer tilt and a dose of 1.6×10^{15} cm^{-2}. The UT-MARLOWE simulation can be available for the calculation of range parameter in molecule BF_2 implanted crystalline silicon. After BF_2 implantation in the silicon, boron and fluorine ions separated from the BF_2 molecule which has a relatively weak bonding energy. The implanted boron profiles were compared with the simulated data as depicted in Fig. 4. UT-MARLOWE simulation matched very well with the SIMS data in 1D, as shown in Fig. 4. The peak of the boron concentration by using SIMS is 5.79×10^{20} cm^{-3} at 0.0177 μm. The comparison from SIMS data and UT-MARLOWE simulation data are shown in Table 3.

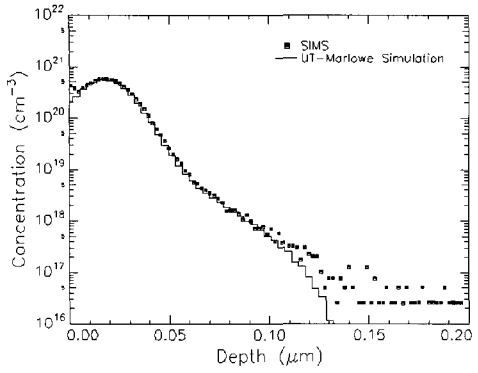

Fig. 4. Boron profiles of BF_2 implanted silicon from the SIMS and the simulation.

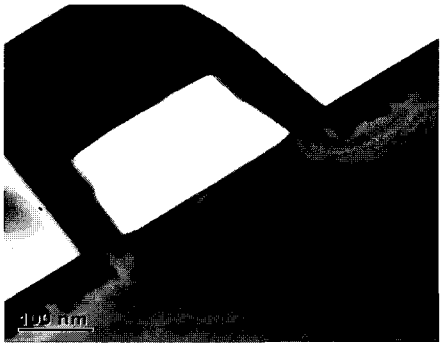

(a) Two-dimensional TEM image

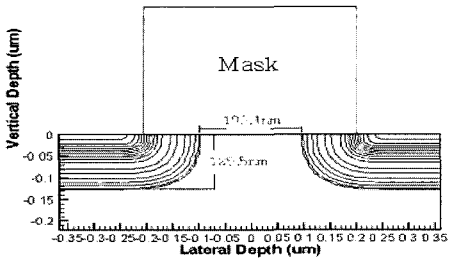

(b) Developed model

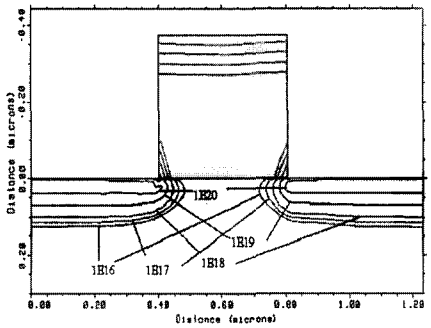

(c) TSUPREM4

Fig. 5. Two-dimensional TEM measured and simulated image of BF_2 implanted silicon after annealing and chemical etching treatment(30,000 × magnification).

Table 4. TEM data after annealing compared with different simulation 2D-data in BF_2 implanted silicon.

Model	Vertical depth (nm)	Channel length (nm)
Developed model	125.5	199.4
TSUPREM4	125.8	233
TEM	125	205

The measured TEM data of the BF_2 implantation were for a channel length and a vertical depth showed 125 nm and 205 nm, respectively. Two-dimensional boron profile is measured by using TEM after annealing process and the magnification of the measured image was 30,000 in Fig. 5. For the electrical activation, annealing processes with furnace were carried out in N_2 gas ambient at 830 °C for 15 min and the simulated boron profiles were compared with the simulated data as depicted in Fig. 5. Under this annealing condition, the boron diffusion coefficient is about 1.421×10^{-16} cm^{-2}/s at 830 °C. The measured boron profile is compared with the simulated data for verification of 2D profiles of the source and the drain. The dark damaged region of the main defects is located at 45 nm in Fig. 5(a).

The boron 2D profiles after chemical etching using 1: 20: 30 mixing solution and 500-W lamp illumination are shown in Fig. 5. Two-dimensional boron profile is measured by using TEM after annealing process and the magnification of the measured image was 30,000 in Fig. 5. The comparison from TEM, TSUPREM4, and developed model are shown in Table 4.

3.2 Two-dimensional implanted arsenic profile through sloped mask structure

20-keV arsenic ions were implanted in silicon at 0 ° wafer tilt and a dose of 3.0×10^{15} cm^{-2}. From the different cases of angle at 60 °, 45 °, and 30 °, the two-dimensional implanted profile through the sloped mask structure is shown in Fig. 6. In the case of 60 °, the channel length is 0.244 μm and vertical depth is 60 nm, respectively and at this vertical depth, the concentration value of doping showed 1.7×10^{16} cm^{-3}. In the case of 45 °, the channel length was 0.212 μm and the vertical depth was 60 nm, respectively. At this vertical depth, the concentration value of doping showed 1.44×10^{16} cm^{-3}. In the case of 30 ° the channel length was 0.2 μm and vertical depth was 60 nm, respectively. At the 60 nm vertical depth, the concentration value of doping showed 1.22×10^{16} cm^{-3}.

From the different mask slope, the concentration-depth profiles due to the vertical direction at x = – 0.165 μm are shown in Fig. 7. In the 30 ° case, the highest

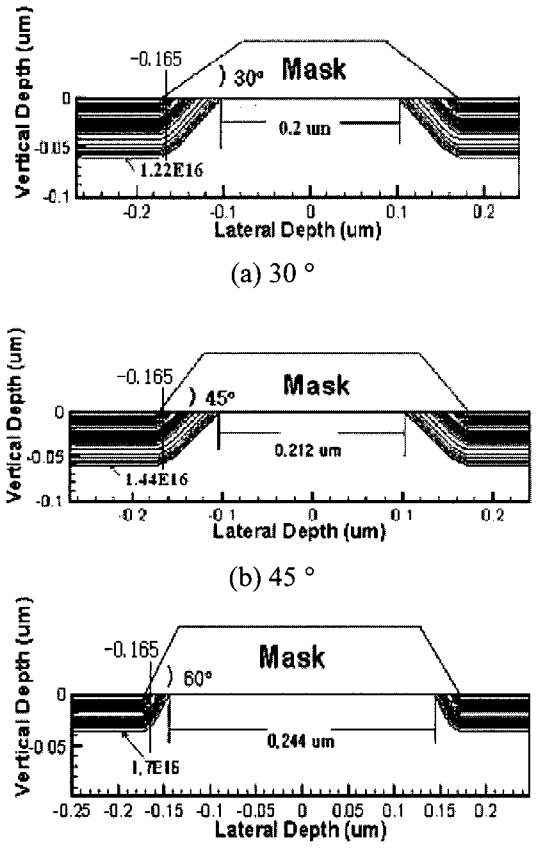

Fig. 6. Two-dimensional implanted arsenic profile through sloped mask structure.

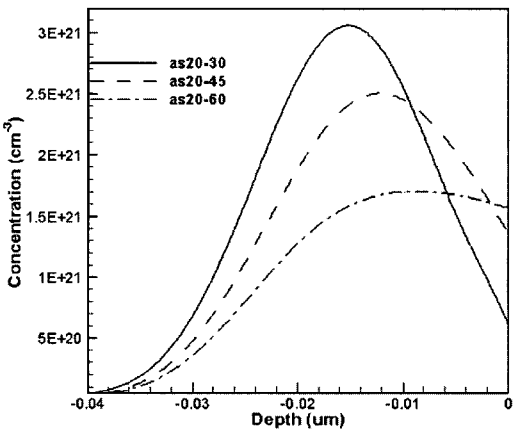

Fig. 7. Profile of arsenic implanted silicon due to vertical direction at x= – 0.165 μm from the Fig. 6.

concentration value was shown from the slow mask structure and conversely, the lowest concentration value was shown from the relatively abrupt mask structure.

4. CONCLUSION

Two-dimensional arsenic and boron profiles in NMOS and PMOS devices for the doping of source and drain were demonstrated by chemical etching-method and with the use of verification through the SRIM, UT-MARLOWE simulation tools and developed model. The measured TEM data and simulation data are shown high correspondence. The etching solution by HF: HNO_3: CH_3COOH (1:20:30) showed best resolution for 2D arsenic and boron profiles and the 2D profiles showed similar Gauss distribution. For better resolution of 2D contour, a 500 W-lamp illuminated the surface of the chemical solution at a distance 15 cm for 10 seconds during the etching. For the arsenic implanted silicon, the vertical depths with the developed model and XTEM data were 79 nm and 83 nm, respectively. The channel lengths with measured XTEM data and developed model were 237 nm and 259 nm, respectively. The TSUPREM4 data for the vertical depth and the channel length were determined to be 85.1 nm and 264.1 nm, respectively. For the BF_2 implanted silicon, the vertical depths with the developed model and XTEM data were 125.5 nm and 125 nm, respectively. The channel lengths with measured XTEM data and developed model were 199.4 nm and 205 nm, respectively. The TSUPREM4 data for the vertical depth and the channel length were determined to be 125.8 nm and 233 nm, respectively. The developed model in this research showed an excellent simulation results as it also matched well with TEM data and TSUPREM4. From the different mask structures with different slope angles, the doping profiles determined with the developed model can be visualized and analyzed. The developed model for the implantation can be used in high energy as well as in low energy. The developed model and XTEM measurements can be used to verify accurately vertical junction depth, lateral depth and channel length in integrated devices.

ACKNOWLEDGMENTS

This work was supported by Kyonggi University Research Grant in the Program Year 2005.

REFERENCES

[1] W. C. Jung, "A study of boron profiles by high energy ion implantation in silicon", J. of KIEEME (in Korean), Vol. 15, No. 4, p. 289, 2002.

[2] W.-C. Jung, "I-V and C-V measurements of fabricated P^+/N^+ junction diode in antimony doped (111) silicon", Trans. EEM, Vol. 3, No. 2, p. 10, 2002.

[3] W.-C. Jung, "A study of experiment and developed model by antimony high energy implantation in silicon", J. of KIEEME(in Korean), Vol. 17, No. 11, p. 1156, 2004.
[4] H. Ruecker, B. Henemann, R. Bath, D. Bolze, V. Melnik, D. Krueger, and R. Kurps, "Formation of shallow source/drain extensions for metal-oxide-semiconductor field-effect", Vol. 82, No. 5, p. 826, 2003.
[5] J. P. Biersack, "Basic physical aspects of high energy implantation", Nucl. Inst. and Meth. B, Vol. 35, p. 205, 1988.
[6] H. H. Andersen and J. F. Ziegler, "Hydrogen, stopping power and ranges in all elements", The Stopping and Ranges of Ions in Matter edited by J. F. Ziegler, Pergamon, New York, Vol. 6, p. 64, 1977.
[7] U. Littmark and J. F. Ziegler, "Handbook of range distributions for energetics ions in all elements", The Stopping and Ranges of Ions in Matter edited by J. F. Ziegler, Pergamon, New York, Vol. 6, p. 45 , 1980.
[8] J. F. Ziegler, "Ion Implantation Science and Technology", Ion Implantation Technology Co., New Jersey, p. 125, 1996.
[9] J. F. Ziegler, "The stopping of energetic light ions in elemental matter", J. Appl. Phys., Vol. 85, No. 3, p. 1249, 1999.
[10] J. F. Ziegler, "SRIM 2000 manual", http://www.srim.org.
[11] J. F. Ziegler, J. P. Biersack, and U. Littmark, "The stopping and range of ions in matter", Vol. 1, New York: Pergamon Press, p. 45, 1985.
[12] K. M. Klein, C. Park, and A. F. Tasch, "Ultra shallow junction formation in silicon using implantation", IEEE Trans. Electron Devices ED Vol. 39, p. 1614, 1992.
[13] A. F. Tasch and S. K. Banerjee, "Ultra shallow junction formation in silicon using ion implantation", Nucl. Inst. and Meth. In Phys. B, Vol. 112, p. 177, 1996.
[14] R. Brindos, P. Keys, K. S. Jones, and M. E. Law, "Effects of arsenic doping on {311} defect dissolution in silicon", Appl. Phys. Letters, Vol. 75, No. 2, p. 229, 1999.
[15] H. Cerva, "Two-dimensional delineation of shallow junctions in silicon by selective etching of transmission electron microscopy cross sections", J. Vac. Sci. Technol. B, Vol. 10, No. 1, p. 491, 1992.
[16] M. A. gribelyuk, M. R. McCartney, J. Li, C. S. Murthy, P. Ronsheim, B. Doris, J. S. McMurray, S. Hegde, and d. J. Smith, "Mapping of electrostatic potential in deep submicron CMOS devices by electron holography", Phy. Rev. Lett., Vol. 89, No. 2, p. 1, 2002.
[17] K. D. Yoo, C. D. Marsh, and G. R. Booker, "Two-dimensional dopant concentration profiles from ultra-shallow junction metal-oxide-semiconductor field-effect transistors using the etch/transmission electron microscopy method", Appl. Phys. Letters, Vol. 80, No. 15, p. 2687, 2002.
[18] Synopsys Inc., "http://www.synopsis.com", TCAD, Taurus TSUPREM4, 2006.
[19] J. D. Plummer, M. D. Deal, and P. B. Griffin, "Silicon VLSI Technology", Prentice Hall, Inc., p. 451, 2000.
[20] R. B. Fair, "The role transient damage annealing in shallow junction formation", Nucl. Instr. and Meth. B, Vol. 37/38, p. 371, 1989.
[21] R. C. Jaeger, "Introduction to Microelectronic Fabrication", Prentice Hall, New Jersey, 2002.
[22] R. P. Webb and E. Maydell, "Comparisons of fast algorithms for calculation of range profiles in layered structures", Nucl. Inst. and Meth. B, Vol. 33 p. 117, 1988.
[23] R. Smith, "Atomic and Ion Collisions in Solids and at Surface", Cambridge University Press, 1997